Toward Cost-Effective and Lightweight Doppler Radars: Papercraft-Based Components and Comparisons With Aluminum and 3-D Printed Alternatives

Anıl Karatay; Enes Ataç; Fatih Yaman

Published version information

Citation: A. Karatay, E. Ataç and F. Yaman, "Toward Cost-Effective and Lightweight Doppler Radars: Papercraft-Based Components and Comparisons With Aluminum and 3-D Printed Alternatives," in IEEE Transactions on Antennas and Propagation, vol. 72, no. 2, pp. 1241-1249, Feb. 2024,

DOI: https://doi.org/10.1109/TAP.2023.3335824

Toward Cost-Effective and Lightweight Doppler Radars: Papercraft-Based Components and Comparisons with Aluminum and 3-D Printed Alternatives

Anıl Karatay, Enes Ataç and Fatih Yaman *

Abstract

Doppler radar systems have an essential role in various applications, including aviation, weather forecasting, and military surveillance. However, their high fabrication costs and heavy weight may limit their utilization in rapid prototyping, small-scale applications, and seamless transportation. To address these challenges, a novel papercraft-based approach for producing the entire Doppler radar system's horn antenna, hybrid tee, and short termination components in the X-band was investigated with details in this study, alongside conventional aluminum and 3D printing methods. This paper presents the first attempt to develop a Doppler radar using papercraft-based manufacturing. The papercraft-based approach is cost-effective, lightweight, flexible, and readily available, offering a promising route for improving and fabricating Doppler radar systems that are both affordable and accessible, particularly in resource-limited settings. The experimental results show that the papercraft-based components can perform comparably to conventional aluminum-based and 3D-printed components, making it an innovative and cost-effective solution for fabricating Doppler radar systems.

radar, antenna, coating, additive manufacturing, papercraft

1 Introduction

Doppler radar systems have become indispensable tools having a wide range of application areas from military surveillance, weather forecasting, and biomedical applications to space exploration and aviation since the detection and measurement of object velocity and motion are critical in today's advanced technology [1–9]. They are capable of detecting and tracking moving objects

*The authors are with the Department of Electrical and Electronics Engineering, İzmir Institute of Technology, Urla, İzmir, 35430 Türkiye. F. Yaman is also with ASTeC, STFC Daresbury Laboratory, WA4 4AD Warrington, United Kingdom. e-mail: anilkaratay@iyte.edu.tr.

by measuring the frequency shift of the electromagnetic waves reflected from the objects. Although traditional Doppler radar systems provide accurate, effective, and high-quality data about events [10, 11], they are often costly and heavy [12], which limits their accessibility and applicability in resource-limited environments and small-scale applications. Recent advancements in fabrication technologies have opened up new opportunities for developing low-cost and lightweight radar systems. Among these, additive manufacturing (AM), called 3D printing, has been increasingly used for producing radar components due to its ability to create high-precision complex shapes and waste reduction [13–18]. However, 3D printing still requires specialized equipment and materials, which may not be available in certain circumstances. Therefore, origami-based components, providing mobility and easy deployment, have received much attention in recent years [19, 20].

Papercraft, is the art of creating three-dimensional objects using paper, has been gaining popularity among hobbyists and artists due to its versatility and accessibility. Its applications extend beyond the realm of art and craft, with papercraft being used in various fields, including architecture, engineering, and even medicine. Although papercraft may incorporate other techniques such as cutting, gluing, and assembly to create more complex and varied forms, it shares many similarities with origami, as it involves the use of paper as a primary material and requires skillful folding techniques to create intricate designs [21]. In recent years, origami techniques have received considerable attention in antenna systems since it is anticipated to have major impact in future communication, sensing, and military applications [22–26]. It provides practical solution for creating low-cost, lightweight, and deployable antennas, which are especially useful for military communication in the microwave frequency range [27–29]. Compared to bulky conventional satellite antennas that require vehicular transport, deployable origami antennas made from paper sheets and conductive tape can be easily carried by military personnel and folded into antennas at desired locations without requiring additional tools. The capability to flatten previously folded structures for reusability, thereby ensuring ease of transportation, and the possibility of re-folding and adhering as needed, emerges as a significant advantage. This makes them a highly attractive option for military applications where mobility and portability are critical [30]. Additionally, origami folding can help to miniaturize antenna size, making them suitable for transportation and easy deployment in various locations. Therefore, the innovative use of papercraft in the fabrication of radar components may also provide a promising solution for creating low-cost, lightweight and accessible radar systems. For instance, their ease of transport and adaptability make them highly valuable in scenarios such as earthquakes, structural collapses, and search missions in remote wilderness areas. On the other hand, on-chip commercially available miniaturized radar sensors are present in the market; however, these systems are not only costly but also highly sophisticated devices from fabrication point of view [31]. Conversely, papercraft-based radar systems maintain a cost below $3, and employ significantly lightweight horn antennas with high gain. By capitalizing on the affordability of both the paper and the conductive tape used as the

coating material, it becomes possible to realize an exceptionally cost-effective radar system [32].

This paper presents a novel approach to microwave component design by proposing and realizing, to the best of our knowledge for the first time, a fully functional complete Doppler radar system operated by papercraft-based components. We mainly focus on three key components of the Doppler radar system: a pyramidal horn antenna, a hybrid tee, and a short termination, excluding the signal generator and detector sections. While horn antennas and rectangular waveguide-based components are preferred for their high gain and low loss, their use as aluminum radar components is constrained by issues of weight, cost, and bulkiness; nevertheless, our papercraft-based approach not only preserves their high range characteristics but also offers solutions to challenges related to weight, cost, and space constraints. A comparative analysis is performed by three different fabrication techniques for producing Doppler radar components: conventional aluminum, 3D printing, and papercraft-based. The aforementioned methods are evaluated in terms of cost, weight, and performance for a complete radar system. The primary objective of our study is to assess the effectiveness of papercraft-based techniques as a credible substitute for conventional fabrication methods in developing affordable, lightweight, and easily accessible Doppler radar systems. The experimental results delve into the viability of integrating papercraft-based components into situations where conventional fabrication techniques, such as resource-limited environments, may not be practical.

The present article is structured as follows. Section II provides a comprehensive overview of the experimental design, encompassing the utilized materials, components, and their fabrication processes employed in the measurements. Section III constitutes the core of the article, where a thorough analysis of the experimental results is presented. Specifically, we compare and contrast the performance of three distinct techniques, evaluating both their strengths and weaknesses. Furthermore, we conduct a detailed S-parameters analysis and provide insightful discussions thereof. Moreover, this section presents the measurement results for the operational radar systems and their comparative analysis, providing a thorough evaluation of these systems. Finally, Section IV offers concluding remarks, summarizing the key findings of the study and highlighting avenues for future research.

2 Materials, Methods and Experimental Designs

In our experiments, the aforementioned components: the pyramidal horn antenna, hybrid tee, and short termination, were configured optimally within the X-band frequency range, specifically at 10 GHz. While the conventional aluminum components required no supplementary treatment, the dielectric materials involved in both 3D printing and papercraft-based approaches are needed to be coated for conductivity. As each 3D printed component is produced as a single piece, spray coating with aerosol provides an effective solution, especially

for tough surfaces such as the inner faces of the hybrid tee. However, the coating process shows differences for the paper-based constituents since exposing the paper to moisture could damage its structure. Therefore, conductive tape is selected as a coating material for paper-based components. The tape has also facilitated the proper establishment of electrical contact between the radar pieces, as it is employed in bonding the grounds of the components.

2.1 Operating principles

The first and simplest component of the Doppler radar, the waveguide-type short termination, consists of a conductive square having reflectivity proportional to the conductivity level. Ideally, an S_{11} value of unity is expected. The second component is the antenna which is a transducer converting electrical signals into electromagnetic waves and vice versa. It is an essential component of radar systems, responsible for transmitting electromagnetic waves into the environment and receiving the reflected waves back from the target. In general, the gain of an antenna is an important measure of the ability to direct the radiation pattern in a particular direction. It plays a critical role in determining the radar's maximum range. The radar range equation is given in Equation 1. It includes the gain of the antenna as a parameter that impacts the radar's maximum range.

$$R = \left(\frac{P_t G^2 \lambda^2 \sigma}{(4\pi)^3 P_{min}} \right)^{\frac{1}{4}} \tag{1}$$

where R: range (m), P_t: transmitted power (W), G: antenna gain (dimensionless), σ: radar cross-section (m^2), λ: wavelength (m) and P_{min}: minimum detectable signal power (W).

The last and most complex component is the hybrid tee. It is a four-port device uses a T-shaped junction with an additional arm to achieve precise and predictable signal division. It is a vital component in microwave and radio frequency systems due to splitting and combining of signals [33]. It operates by splitting an input signal (Port 3 in Fig. 1) equally between two ports (Port 1 and Port 2) and, conversely, combining signals from two ports to the input port. It has high isolation level between the input port and the additional arm (Port 4). It offers wide-ranging functionality and ability to deliver high-performance results. Moreover, its ability to act as a mixer combining transmitted and received signals makes it one of the most critical components in Doppler radar systems.

The scattering matrix, called S-matrix, represents the relation between the initial and final states of a physical system in a reflection mechanism which can be expressed as Equation 2 [34] for an ideal hybrid tee. In this context, an input signal at frequency f_0 given from the third port is equally divided between the first and second ports. The signal transmitted to the first port is terminated with a short circuit, causing it to be fully reflected with a frequency of f_0. The second port contains an antenna, and if there is a moving object in front of it, the signal reflected from the object will be shifted in frequency by the Doppler

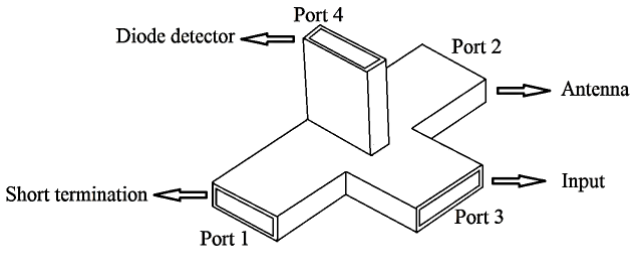

Figure 1: Configuration of the radar and port numbers of the hybrid tee

effect to $f_0 \pm f_d$. As a result, the first and second ports will provide simultaneous input power to the system.

$$\begin{bmatrix} S_{11} & S_{12} & S_{13} & S_{14} \\ S_{21} & S_{22} & S_{23} & S_{24} \\ S_{31} & S_{32} & S_{33} & S_{34} \\ S_{41} & S_{42} & S_{43} & S_{44} \end{bmatrix} = \begin{bmatrix} 0 & 0 & \frac{1}{\sqrt{2}} & \frac{1}{\sqrt{2}} \\ 0 & 0 & \frac{1}{\sqrt{2}} & -\frac{1}{\sqrt{2}} \\ \frac{1}{\sqrt{2}} & \frac{1}{\sqrt{2}} & 0 & 0 \\ \frac{1}{\sqrt{2}} & -\frac{1}{\sqrt{2}} & 0 & 0 \end{bmatrix} \tag{2}$$

Assuming that the third and fourth ports are completely isolated, the factor determining the signal that will be observed at the fourth port is the signals entering the system from the first and second ports. If we call the voltage wave transferred from the first port to the system as A and the one entering from the second port as B, the value observed at the fourth port will be $\frac{1}{\sqrt{2}}(A-B)$. After the vector sum/difference of signals at two different frequencies is obtained by the hybrid tee, the diode detector at the output of the fourth port can provide the user with the intermediate frequency of f_d. As the diode detector operates as an envelope detector, it can be employed to detect the low-frequency signal component of two distinct signals, such as a carrier signal and its modulating message signal.

The velocity equation in a Doppler radar can be expressed using the transmitted frequency f_0 and the received Doppler frequency f_d. Assuming that the radar is stationary, the frequency shift f_d observed in the received signal is due to the Doppler effect caused by the movement of the target object. The longitudinal velocity of the object relative to the radar can be calculated using the following equation [35]:

$$v = \frac{cf_d}{2f_0} \tag{3}$$

where c is the speed of light.

2.2 Experimental Design and Fabrication

In this subsection, three specific components were meticulously scrutinized in the pursuit of creating each individual radar structure. The designed pyramidal

horn antenna has an aperture area of $96 \times 73\ mm^2$ and a height of 120 mm. The dimensions of the waveguide attached to the horn antenna have been determined as $22.86 \times 10.16 \times 40\ mm^3$. The length of the waveguide between the first and second port of the hybrid tee, which has the same cross-sectional area, is 70 mm, while the lengths of the other two extensions are 35 mm. The short termination is a square structure with a cross-sectional area of $40 \times 40\ mm^2$.

The initial technique employed in manufacturing these radar components involves aluminum-based production, a widely recognized methodology realized through machining. In contrast, the alternative technique utilized in this study consists of producing 3D-printed radar components, which were generated by exporting STL files of appropriate dimensions for direct replication. The structures, created utilizing a dielectric material known as PLA, were subsequently given conductivity by applying a conductive spray coating to the interior surfaces. However, the primary innovation highlighted in this article involves creating paper-based radar components and the subsequent assembly of these components to form an operational Doppler radar structure. This was accomplished meticulously, whereby each of the three components was cut from a suitably thick and foldable paper before being coated with conductive adhesive tape. The paper was then precisely folded along predetermined lines and, if necessary, subjected to cutting and gluing procedures. Detailed information on the precise steps involved in this process is provided in the accompanying figures.

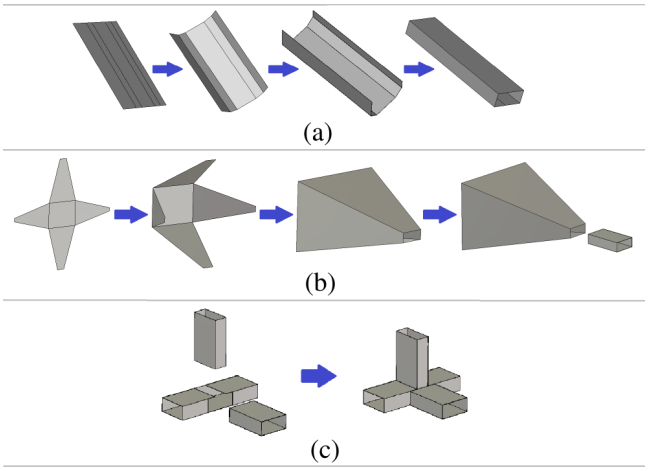

Figure 2: Manufacturing of the papercraft-based components in the X-band (a) waveguide (b) pyramidal horn antenna (c) hybrid tee

The illustration in Fig. 2-(a) shows steps to produce an X-band waveguide, relying on the intricacies of papercraft. The waveguide comprises five parts, consisting of four edges and a singular ear, and each is carefully cut to conform to the prescribed dimensions and subsequently covered with conductive tape

whose electrical conductivity is approximately 20000 S/m [32]. Post-covering, the thick paper is marked and folded to manifest the intended structure, which is then securely affixed using adhesive and conductive tape. The easily foldable thick paper, having the ability to distribute stress across its surface, possesses a Young's Modulus ranging from 1 to 4 GPa [36]. If necessary, flanges belonging to the corresponding structure are also cut and conductive before being added to the end of the produced waveguide.

Fig. 2-(b) depicts the proposed production process for a pyramidal horn antenna. Similarly to the previous example, the paper is precisely cut to the appropriate size and shape, covered with conductive tape, and subsequently folded to achieve the desired incised pyramid shape. After the folded segments are adjoined together, they are glued with the waveguide produced using the recommended method from the previous step to acquire the final form. Once the gluing is finalized, the lower section of the incised pyramid, which comprises the mouth of the horn antenna, is meticulously trimmed to yield an open pyramidal horn antenna structure, tailor-made to meet the specific requirements of the application at hand.

Lastly, for producing a hybrid tee, three rectangular waveguides, one measuring 7 cm and the others 3.5 cm in length, are meticulously aligned to create the basic structure. From the center of the 7 cm waveguide, a curved T-shaped section is cut to conform to the other two waveguides precisely. Subsequently, the waveguides are adjoined using the papercraft-based method, as depicted in Fig. 2-(c). Then, the flanges are affixed to the outputs of the waveguides, thus concluding the production process of the papercraft-based hybrid tee. In producing a short termination, a square with a cross-sectional area of 4×4 cm^2 is cut, and at least one of its sides are covered with conductive tape. In our study, both surfaces were covered with conductive tape to increase the level of insulation and enhance the durability of the paper-based structure.

3 Results and Discussions

This section is dedicated to compiling and interpreting the measurement results of the short terminations, horn antennas, and hybrid tee components, which have been produced using three different fabrication methods, and combining them to form a constructed radar. Each of the produced components' S-parameters were individually measured using HP 8720D 50 MHz-20 GHz vector network analyzer (VNA), and the gain and pattern results for the antenna were analyzed in an anechoic chamber. Additionally, by combining the radar structures with a signal generator and detector, velocity information about a moving target was obtained.

3.1 Characterization of the components

In this subsection, results are presented for S-parameter measurements of components obtained through the various production methods, as well as gain and

pattern measurements for antennas. Fig. 3 displays nine different components, each produced through one of three distinct methods: aluminum, 3D printing, and papercraft-based manufacturing. The aluminum components are located at the bottom left of the triangular arrangement, the 3D-printed components at the bottom right, and the papercraft-based replicas at the apex of the triangle. In Fig. 4, S_{11} results are presented for short terminations and horn antennas produced using various fabrication techniques. Initially, aluminum, 3D printed, and papercraft-based shorts were screwed onto the coaxial to waveguide adapter at the output of the VNA, and S_{11} values were examined in the 6-15 GHz range. Based on these results, the reflection coefficient values of all three components are very close to 0 dB, indicating that the short terminations effectively fulfill their intended function. Following this, the same process was executed to the horn antenna, and S_{11} values were investigated in the same frequency range. The S_{11} parameter for all three components, which descended below -6 dB at 8 GHz, did not ascend above -6 dB again across the evaluated frequency band. Notably, at the operational frequency of the radar, 10 GHz, the S_{11} value for all three components was beneath -10 dB, indicating that all three antennas were adequately successful in terms of impedance matching. To put it differently, this graphical representation reveals that the papercraft-based horn antenna, when compared to other costly, time-consuming, and logistically challenging alternatives, delivers a similar level of efficacy with respect to impedance matching. Photographs depicting the antennas during the scattering parameter measurement are presented in Fig. 5.

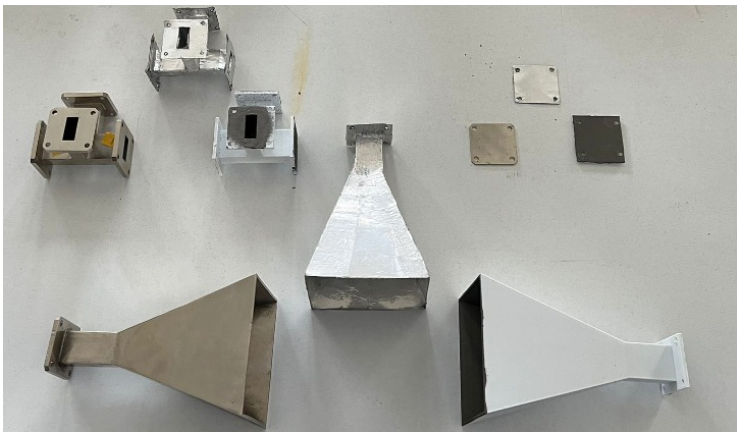

Figure 3: Hybrid tee, pyramidal horn and short termination manufactured with three different fabrication methods

The measurements of the realized gain and far field patterns of the antennas were performed in an anechoic chamber. The realized gain values for aluminum, 3D printed, and paper-based antennas at 10 GHz were measured as 18.1, 17.5, and 16.5 dBi, respectively. In this regard, the results suggest that the paper-based antenna is not only impedance-matched but also offers comparable

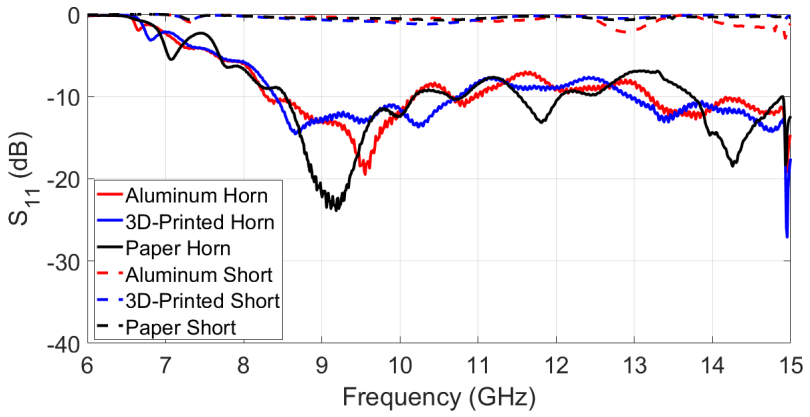

Figure 4: S_{11} results of horn antennas and short terminations for three different manufacturing methods

(a) (b) (c)

Figure 5: VNA measurements of the horn antennas (a) Aluminum (b) 3D printed (c) Papercraft-based

performance in gain to its aluminum and 3D printed counterparts, thereby underscoring its suitability for deployment in practical applications. The results of the normalized far field pattern and the photographs taken during the pattern measurements in the anechoic chamber for horn antennas are showcased in Fig. 6 and 7. As shown in Fig. 6-(a) and -(b), the normalized H- and E-plane far field pattern results are approximately the same for all three manufacturing methods. Here, the term H-plane refers to the azimuthal axis when the longer side of the horn antenna is parallel to the ground, while the term E-plane pertains to the pattern information regarding the azimuthal axis when the shorter side of the horn antenna is parallel to the ground. Although there are minor differences visible in the side angles of the antennas due to differences in conductivity levels, the overall behavior of the three antennas is quite similar to each other. Using the CST software, the conductivity-dependent variation in

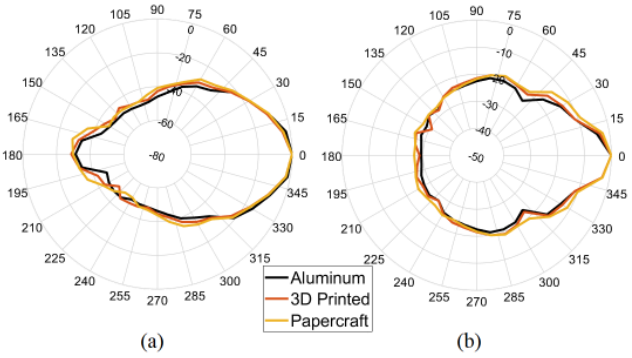

Figure 6: Pattern measurements of the horn antennas manufactured with various methods (a) Normalized H-plane results (b) Normalized E-plane results

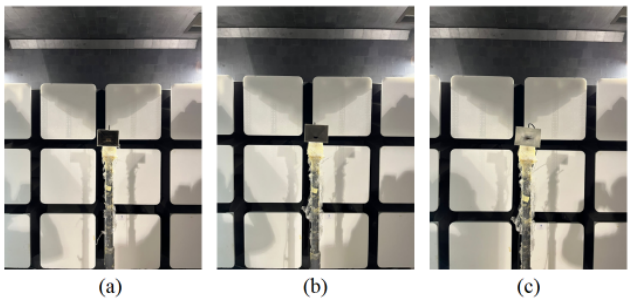

Figure 7: Pattern measurements photos of the horn antennas in the anechoic chamber (a) Aluminum horn antenna (b) 3D printed horn antenna (c) Papercraft-based horn antenna

the gain of the X-band horn antenna was simulated for three different frequencies, and the results are presented in Fig. 8. According to this simulation, the known conductivity level of approximately 20000 S/m for the conductive tape, does not exhibit a significantly adverse impact on the antenna's performance. The manifestation of this negative effect is observed when the conductivity level is reduced to approximately below 500 S/m.

Following the initial measurements of the short terminations and horn antennas, the subsequent step involved conducting S-parameter measurements for three different hybrid tees. As a passive and reciprocal component with four ports, the hybrid tee requires a total of ten graphs to be properly characterized, including S_{11}, S_{22}, S_{33}, S_{44}, S_{21}, S_{31}, S_{41}, S_{32}, S_{42}, and S_{43}. However, the excessive number of graphs involved and the potential to clutter the article's presentation necessitated a judicious approach to combining certain scattering parameters into a single figure, thereby optimizing the readability and coherence of the data. By virtue of symmetry, one anticipates that the S_{11} and S_{22} parameters would be equivalent. Similarly, the instances where $S_{31} = S_{32}$ and

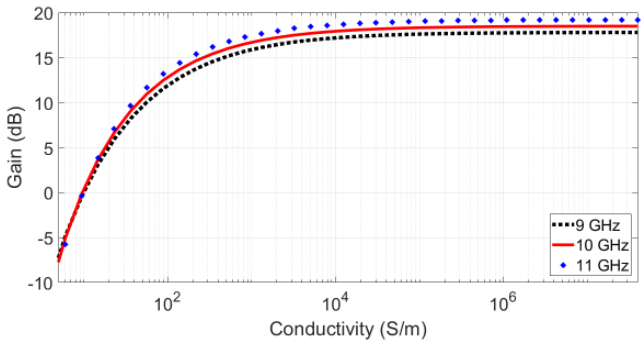

Figure 8: Simulation results of gain versus conductivity for X-band horn antenna

$S_{41} = S_{42}$ are also envisaged. As depicted in Fig. 9, the S-parameter measurements of the papercraft-based hybrid tee yielded results that are comparable to those of its aluminum and 3D printed counterparts, thus demonstrating its suitability for utilization in a radar system. The outcomes evince the requisite precision of the fabrication process. The measurements illustrate that the short termination, horn antenna, and hybrid tee components produced using metalized foldable papers with a conductive tape exhibit performance that is comparable to that of their aluminum-based counterparts, which are notably more costly and heavy.

3.2 Doppler radar measurements

This subsection presents the results of Doppler radar measurements and a comparative analysis of three different Doppler radar structures. Each structure was constructed using a combination of aluminum, 3D printed, and papercraft-based components. The first and second ports of the hybrid tee were terminated with short loads and pyramidal horn antennas, while the third and fourth ports were utilized as input and output ports. These ports were terminated to carry out the test measurements using Amitec X-band Gunn oscillator and X-band matched envelope detector, both operating within the 8-12 GHz range. Given the symmetrical nature of the first and second ports, the specific allocation of the short load and antenna to each port is inconsequential. Fig. 10 illustrates that short loads and antennas were connected to the first two ports of the hybrid tee for each of the three distinct manufacturing methods, while the third and fourth ports were left unconnected for the attachment of signal generators and detectors.

Before proceeding to radar measurements, it is crucial to precisely tune the operating frequency of the radar to the desired frequency. The operating frequency must be measured with great accuracy since it is also utilized in the subsequent velocity calculation. Given that our signal source lacks a frequency display option, we placed an additional X-band horn antenna and a spectrum analyzer connected to it in front of the radar during operation to adjust the

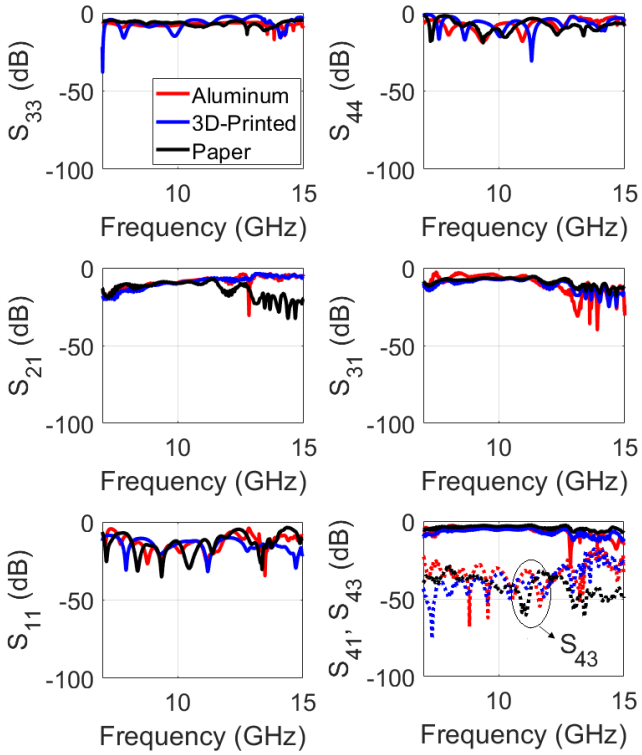

Figure 9: S parameters of the hybrid tees for three different manufacturing methods

operating frequency of the radar precisely. As depicted in Fig. 11-(a), the operating frequency of the radar was measured to be 10 GHz. In the radar measurements, two different measurement scenarios were focused on for three different configurations. In the first scenario, measurement sets of a person who started walking towards the radar around the fifth second and after waiting near the radar for a short period, walked back in the opposite direction. The second scenario includes the measurement sets of a pendulum placed directly in front of the radar and a metal ball attached to the end of this pendulum. A photograph of the pendulum measurement can be seen in Fig. 11-(b). These scenarios were utilized to evaluate the performance of the radar system in detecting moving objects and to assess its ability to measure the velocity of those objects accurately.

The measurement results for the first scenario are presented in Fig. 12. These three figures show the measurements for the Doppler radar structures made of aluminum, 3D printed components, and papercraft-based materials, respectively. A person who starts walking towards the radar from a distance of a few meters waits for approximately 4 seconds after approaching the radar and

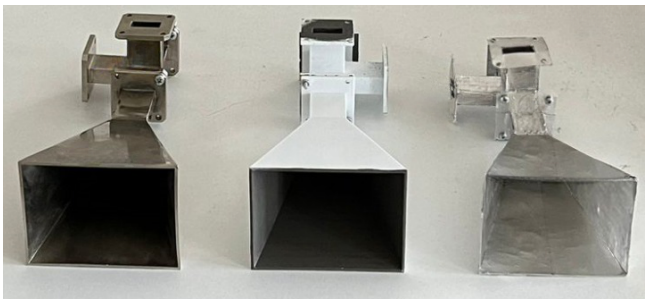

Figure 10: Assembled Doppler radar configuration manufactured with three different fabrication methods: Aluminum, 3D printed and papercraft-based

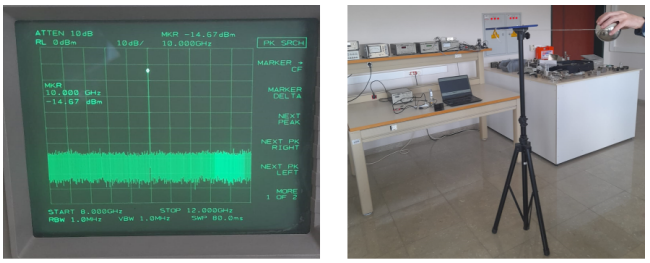

(a) (b)

Figure 11: Doppler radar measurement (a) Operating frequency of the Doppler radar (b) A photograph of the pendulum experiment

then walks back in the opposite direction. When considering parameters such as distance and arrival time between the radar and the starting point, it can be observed that the velocity of the person matches the radar result. The yellow colors in the figures indicate an increase in the power level, while the blue colors indicate a decrease.

The papercraft-based approach was measured on the same scale as the other two cases, and it was found that the SNR value of the proposed approach was lower than the other two configurations. Several factors may contribute to the higher noise levels observed in the papercraft-based approach compared to the other two configurations at the same scale. Firstly, the antenna gain is lower in the papercraft-based design. Secondly, the durability of the magic tee structure is lower in the papercraft-based approach compared to the other two, leading to micro deformations. Thirdly, the coating material used in the papercraft-based approach exhibits higher losses. Finally, the micro misalignment of the input and output ports of the papercraft-based components contributes to higher noise levels.

To observe the velocity measurement in a more controlled manner, a pendulum was placed 1.5 m in front of the radar structures, and the velocity graph of the metal ball at the end of the pendulum was plotted in Fig. 13. The maximum

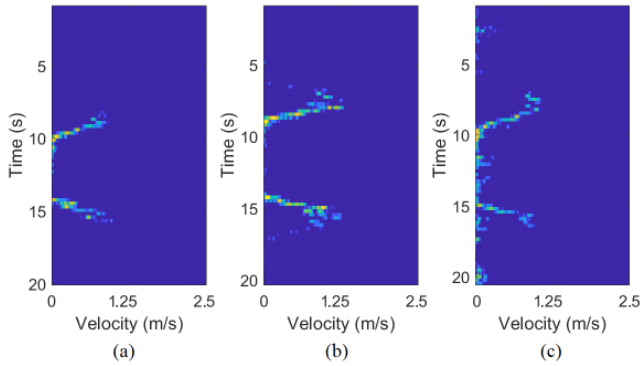

Figure 12: Doppler radar results of a walking person with (a) Aluminum components (b) 3D printed components (c) Papercraft-based components

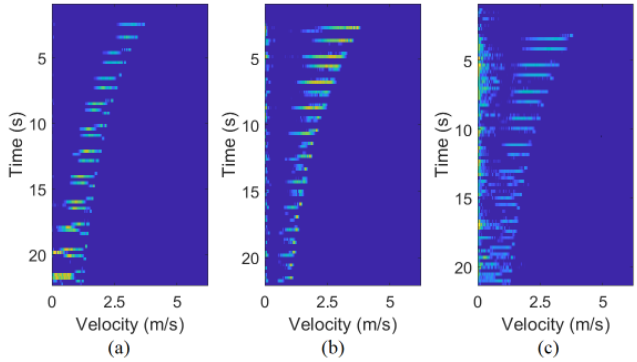

Figure 13: Doppler radar results of a pendulum with (a) Aluminum components (b) 3D printed components (c) Papercraft-based components

velocity of the pendulum, hanging from a one-meter string, was measured at approximately 4 m/s in the first swing for all three configurations. This velocity decreased in accordance with the pendulum equation, yielding approximately the same result for all configurations. In this measurement, as in the walking person experiment, the noise level was slightly higher in the papercraft-based method than in the other two methods. To determine the relative Signal-to-Noise Ratio (SNR) levels in a quantitative manner, the variations in SNR between three different manufacturing techniques were determined using distances corresponding to minimum detectable power levels, through the radar range equation. In the measurements conducted with reference to an aluminum-based radar, the SNR of the 3D printed radar was found to be approximately 2 dB lower than that of the aluminum-based radar, while the SNR of the papercraft-based radar was about 1.5 dB less than that of the 3D printed radar. However, the ultra-cost-effectiveness, extreme lightness, seamless transportation, and ease

of accessibility provided by the papercraft-based approach make it a tolerable disadvantage. It should also be noted that these results represent the first successful attempt to obtain a Doppler radar using a papercraft-based approach.

Table 1: Comparison of the various manufacturing methods of the radar systems

	Aluminum	3D Printed	Paper
Cost	$\sim$ \$400	$\sim$ \$40	$\sim$ \$3
Weight	801 g	99 g	34 g
Manufacturing time	$\sim$ 4-6 hours	$\sim$ 1 day	$\sim$ 1-2 hours
Range (10 mW input)	10 m	9 m	8 m
Durability	High	Medium	Low

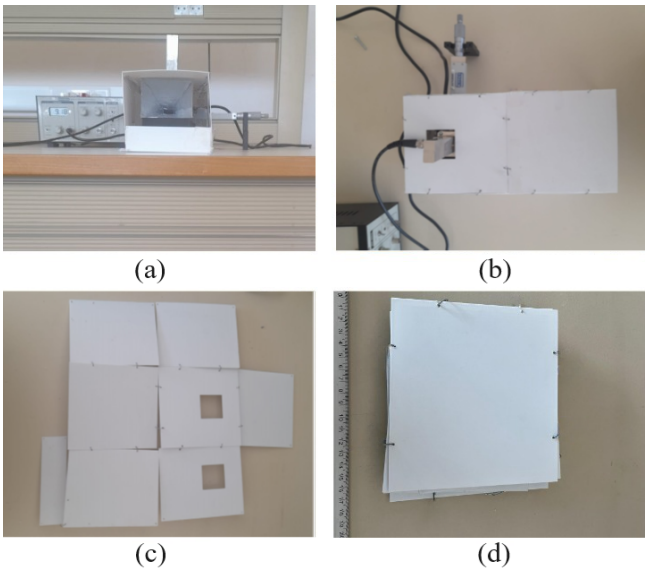

Figure 14: A weatherproof enclosure (a) Operational form with radar (b) overhead view (c) flattened form (d) folded form

In Table 1, a comparison of the cost, weight, performance and manufacturing time of aluminum, 3D printed, and paper-based radars is provided. In terms of cost, aluminum radar components are the most expensive option, whereas the cost burden is greatly reduced with 3D-printed components. However, it is a fact that the 3D printing service or the device that produces it is still considerably more expensive than paper-based materials. On the other hand, the ability of components produced particularly at high frequencies, such as X-band, to be coated with conductive materials like conductive tape when produced as a single piece is quite weak, necessitating the need for a conductive aerosol coating method, which is a more expensive alternative to conductive tape. If

the 3D printed components are produced in several pieces to be coated with conductive tape, they become much more lossy due to the gaps that will be left in between. The weight comparison also yields a result in line with the cost. The required durations for production methods vary; particularly, when considering the necessity for aerosol coating of the 3D-printed structure, the drying time can extend up to one day. On the other hand, the production times for aluminum structures that need to undergo machining and grinding processes are both complex, requiring sophisticated machinery, and longer compared to the papercraft-based structures. The paper-based approach is far ahead of the other two methods in terms of both weight and portability. Despite the fact that the range of the paper-based radar is lower than the other two approaches due to the conductivity difference and minor deformations of the paper, this difference is bearable in comparison to the advantages it provides. Here, the given ranges in Table I indicate the maximum achievable distances with 10 mW input power. The main disadvantage of the paper-based approach appears to be durability. Although there is no serious problem regarding its use in a closed or isolated area, its use may be limited in areas exposed to rain and wind, but this problem can be overcome with different types of paper, new coating methods or employing radomes.

In the last step, a weatherproof enclosure using plastic material for the proof of concept was constructed to improve the durability of the radar. This not only protects the radar from the weather conditions but also shields it from physical damage and attacks at a certain level. The enclosure is designed to have a foldable structure to maintain the portability of the papercraft-based Doppler radar. In this context, it is achieved by assembling eight thin sheets in a foldable manner. To avoid impacting the radar's performance, the aperture of the horn antenna is left open when it is operational. Additionally, two square-shaped apertures are introduced to facilitate the placement of the oscillator and the detector. Thus, it has been demonstrated that the proposed papercraft-based structure can be used in conjunction with a portative and foldable protective cover without compromising its ease of portability.

4 Conclusion

The present study showcases a novel approach in the field of radar technology by successfully designing and testing a Doppler radar system composed of papercraft-based components. The hybrid tee, pyramidal horn, and short termination are among the components constructed through this approach, with the exception of the signal generator and detector. This accomplishment marks the first fully functional Doppler radar system where all essential components are made from papercraft-based approaches, highlighting the innovation of this research. This unconventional and inventive technique not only confirms the feasibility of using papercraft as an affordable and lightweight substitute for traditional materials in radar components but also provides a new perspective on the development of radar systems. The study also offers valuable insights for

future research by comparing the cost, weight, and performance of three different manufacturing methods: conventional aluminum, 3D printing, and papercraft-based approaches. The antennas, which has similar realized gain values measured as 18.1, 17.5, and 16.5 dBi, and other components with S-parameters that are also found to be quite close to each other, do not exhibit a significant difference in performance. The measured weights are found to be 801 g, 99 g, and 34 g, respectively, which will yield substantial benefits in the production of larger-scale or larger-sized components with a range loss of merely 20%. This approach would be more effective at low frequencies rather than X-band, as the deformations caused by paper and conductive tape are relatively reduced at low frequencies, including the emergence of more noticeable differences in the weight and cost comparison of the systems. Furthermore, the proposed system presents high potential for diverse applications in numerous fields, such as remote sensing and target detection in some military applications and search missions owing to its simplicity, low cost, effortless transportation, and versatility. The papercraft-based approach additionally introduces new prospects for the creation of other electronic components with comparable characteristics. In summary, we believe the design and development of a papercraft-based Doppler radar system is a remarkable contribution to the radar technology, as it emphasizes the potential of unconventional materials and fabrication methods in the development of alternative microwave components.

References

[1] Y. He, C. Gu, H. Ma, J. Zhu, and G. V. Eleftheriades, "Miniaturized circularly polarized Doppler radar for human vital sign detection," *IEEE Transactions on Antennas and Propagation*, vol. 67, no. 11, pp. 7022–7030, 2019.

[2] B. L. Cheong, R. Kelley, R. D. Palmer, Y. Zhang, M. Yeary, and T.-Y. Yu, "Px-1000: A solid-state polarimetric X-band weather radar and time–frequency multiplexed waveform for blind range mitigation," *IEEE Transactions on Instrumentation and Measurement*, vol. 62, no. 11, pp. 3064–3072, 2013.

[3] M. Nosrati and N. Tavassolian, "Effects of antenna characteristics on the performance of heart rate monitoring radar systems," *IEEE Transactions on Antennas and Propagation*, vol. 65, no. 6, pp. 3296–3301, 2017.

[4] W. Xia, Y. Li, and S. Dong, "Radar-based high-accuracy cardiac activity sensing," *IEEE Transactions on Instrumentation and Measurement*, vol. 70, pp. 1–13, 2021.

[5] G. T. Capraro, A. Farina, H. Griffiths, and M. C. Wicks, "Knowledge-based radar signal and data processing: a tutorial review," *IEEE Signal Processing Magazine*, vol. 23, no. 1, pp. 18–29, 2006.

[6] R. J. Doviak *et al.*, *Doppler radar and weather observations*. Courier Corporation, 2006.

[7] Y. Kim, S. Ha, and J. Kwon, "Human detection using doppler radar based on physical characteristics of targets," *IEEE Geoscience and Remote Sensing Letters*, vol. 12, no. 2, pp. 289–293, 2014.

[8] C. Li, V. M. Lubecke, O. Boric-Lubecke, and J. Lin, "A review on recent advances in Doppler radar sensors for noncontact healthcare monitoring," *IEEE Transactions on Microwave Theory and Techniques*, vol. 61, no. 5, pp. 2046–2060, 2013.

[9] Y. S. Lee, P. N. Pathirana, C. L. Steinfort, and T. Caelli, "Monitoring and analysis of respiratory patterns using microwave doppler radar," *IEEE Journal of Translational Engineering in Health and Medicine*, vol. 2, pp. 1–12, 2014.

[10] A. Karatay, D. Orcan, C. Özkal, and F. Yaman, "Implementation and experimental verifications of microstrip antennas for angular scanning of a Doppler radar," *AEU-International Journal of Electronics and Communications*, vol. 101, pp. 76–84, 2019.

[11] M. Yeary, B. L. Cheong, J. M. Kurdzo, T.-Y. Yu, and R. Palmer, "A brief overview of weather radar technologies and instrumentation," *IEEE Instrumentation & Measurement Magazine*, vol. 17, no. 5, pp. 10–15, 2014.

[12] H. Ö. Yılmaz and F. Yaman, "Metamaterial antenna designs for a 5.8-ghz Doppler radar," *IEEE Transactions on Instrumentation and Measurement*, vol. 69, no. 4, pp. 1775–1782, 2019.

[13] Z. Cai, Y. Zhou, Z. Weng, L. Deng, Y. Luo, M. Yu, and Y. Qi, "3-D printing conformal K-band lens antenna for a smart parking space detection system," *IEEE Transactions on Instrumentation and Measurement*, vol. 69, no. 10, pp. 8514–8525, 2020.

[14] M. Liang, J. Wu, X. Yu, and H. Xin, "3D printing technology for RF and THz antennas," in *2016 International Symposium on Antennas and Propagation (ISAP)*. Ieee, 2016, pp. 536–537.

[15] H. Yao, S. Sharma, R. Henderson, S. Ashrafi, and D. MacFarlane, "Ka band 3D printed horn antennas," in *2017 Texas Symposium on Wireless and Microwave Circuits and Systems (WMCS)*. IEEE, 2017, pp. 1–4.

[16] J. Wu, C. Wang, and Y. Guo, "Ridged waveguide magic tees based on 3-D printing technology," *IEEE Transactions on Microwave Theory and Techniques*, vol. 68, no. 10, pp. 4267–4275, 2020.

[17] P. Njogu, B. Sanz-Izquierdo, A. Elibiary, S. Y. Jun, Z. Chen, and D. Bird, "3D printed fingernail antennas for 5G applications," *IEEE Access*, vol. 8, pp. 228 711–228 719, 2020.

[18] D. Helena, A. Ramos, T. Varum, and J. N. Matos, "Antenna design using modern additive manufacturing technology: A review," *IEEE Access*, vol. 8, pp. 177 064–177 083, 2020.

[19] S. I. H. Shah, S. Bashir, M. Ashfaq, A. Altaf, and H. Rmili, "Lightweight and low-cost deployable origami antennas—A review," *IEEE Access*, vol. 9, pp. 86 429–86 448, 2021.

[20] A.-S. Kaddour, C. L. Zekios, and S. V. Georgakapoulos, "A reconfigurable origami reflectarray," in *2020 14th European Conference on Antennas and Propagation (EuCAP)*. IEEE, 2020, pp. 1–4.

[21] J. J. Park, P. Won, and S. H. Ko, "A review on hierarchical origami and kirigami structure for engineering applications," *International Journal of Precision Engineering and Manufacturing-Green Technology*, vol. 6, pp. 147–161, 2019.

[22] G. J. Hayes, Y. Liu, J. Genzer, G. Lazzi, and M. D. Dickey, "Self-folding origami microstrip antennas," *IEEE Transactions on Antennas and Propagation*, vol. 62, no. 10, pp. 5416–5419, 2014.

[23] S. V. Georgakopoulos, "Reconfigurable origami antennas," in *2019 International Applied Computational Electromagnetics Society Symposium (ACES)*. IEEE, 2019, pp. 1–2.

[24] S. V. Georgakopoulos, C. L. Zekios, A. Sattar-Kaddour, M. Hamza, A. Biswas, B. Clark, C. Ynchausti, L. L. Howell, S. P. Magleby, and R. J. Lang, "Origami antennas," *IEEE Open Journal of Antennas and Propagation*, vol. 2, pp. 1020–1043, 2021.

[25] S. I. H. Shah and S. Lim, "A dual band frequency reconfigurable origami magic cube antenna for wireless sensor network applications," *Sensors*, vol. 17, no. 11, p. 2675, 2017.

[26] J. Kimionis, M. Isakov, B. S. Koh, A. Georgiadis, and M. M. Tentzeris, "3D-printed origami packaging with inkjet-printed antennas for RF harvesting sensors," *IEEE Transactions on Microwave Theory and Techniques*, vol. 63, no. 12, pp. 4521–4532, 2015.

[27] S. I. H. Shah, M. M. Tentzeris, and S. Lim, "Low-cost circularly polarized origami antenna," *IEEE Antennas and Wireless Propagation Letters*, vol. 16, pp. 2026–2029, 2017.

[28] S. I. H. Shah, S. Lim, and M. M. Tentzeris, "Military field deployable antenna using origami," in *2017 International Workshop on Antenna Technology: Small Antennas, Innovative Structures, and Applications (iWAT)*. IEEE, 2017, pp. 72–73.

[29] A. Thrall and C. Quaglia, "Accordion shelters: A historical review of origami-like deployable shelters developed by the US military," *Engineering Structures*, vol. 59, pp. 686–692, 2014.

[30] S. I. H. Shah and S. Lim, "Review on recent origami inspired antennas from microwave to terahertz regime," *Materials & Design*, vol. 198, p. 109345, 2021.

[31] T. Instruments. (Accessed 2023) mmWave radar sensors. [Online]. Available: https://www.ti.com/sensors/mmwave-radar/overview.html

[32] A. Karatay, H. Ö. Yılmaz, C. Özkal, and F. Yaman, "Cost-effective experiments with additively manufactured waveguide and cavities in the S-band," *Measurement Science and Technology*, vol. 34, no. 8, p. 085904, 2023.

[33] U. Barabas, "On an ultrabroad-band hybrid tee," *IEEE Transactions on Microwave Theory and Techniques*, vol. 27, no. 1, pp. 58–64, 1979.

[34] D. M. Pozar, *Microwave Engineering*. John wiley & sons, 2011.

[35] M. I. Skolnik, *Radar Handbook*. McGraw-Hill Education, 2008.

[36] E. Filipov, K. Liu, T. Tachi, M. Schenk, and G. H. Paulino, "Bar and hinge models for scalable analysis of origami," *International Journal of Solids and Structures*, vol. 124, pp. 26–45, 2017.